

Effect of grain refinement by severe plastic deformation on the next-neighbor misorientation distribution

L.S. Tóth^{a,*}, B. Beausir^b, C.F. Gu^c, Y. Estrin^{c,d}, N. Scheerbaum^b, C.H.J. Davies^c

^a *Laboratoire d'Etude des Microstructures et de Mécanique des Matériaux (LEM3), Université Paul Verlaine – Metz/CNRS, 57045 Metz, France*

^b *Institut für Strukturphysik, Technische Universität Dresden, D-01062 Dresden, Germany*

^c *Department of Materials Engineering, Monash University, Clayton, VIC 3800, Australia*

^d *CSIRO Division of Process Science and Engineering, Clayton, VIC, Australia*

Received 6 August 2010; received in revised form 25 August 2010; accepted 26 August 2010

Available online 21 September 2010

Abstract

Next-neighbor misorientation distributions (NNMD) in severely deformed polycrystalline materials are commonly measured by orientation imaging. A procedure is proposed which enables the separation of NNMD of ultrafine-grained materials into two parts: the distribution of misorientations between newly emerged grains within the original (“parent”) grain interior (“internal daughter grains”) and the distribution of misorientations between grains adjacent to an original grain boundary on its opposite sides (“grain boundary daughter grains”). The procedure is based on electron backscatter diffraction orientation map analyses carried out on different planes of deformed samples considering the evolution of the grain size and shape during severe plastic deformation. It was applied to copper processed by up to three passes of equal-channel angular pressing. A characteristic feature of the measured NNMD is the occurrence of a double peak, which is clearly due to the differences between the NNMD of the two distinct populations of new grains defined above. The peak at low angles represents mainly the continual grain subdivision process in the interior of a parent grain (and is associated with internal daughter grains), while the peak at large angles is due to the high angle misorientations of the grain boundary daughter grains.

© 2010 Acta Materialia Inc. Published by Elsevier Ltd. All rights reserved.

Keywords: Misorientation; Ultrafine-grained; Equal-channel angular pressing; Electron backscatter diffraction; Severe plastic deformation

1. Introduction

Grain refinement achieved by applying large plastic strains is one of the main reasons why severe plastic deformation (SPD) processes have attracted much interest in recent years. Among the most popular SPD techniques, equal-channel angular pressing (ECAP) takes a special place, mainly because it offers the possibility of producing bulk ultrafine-grained materials in a relatively easy way [1]. The grain refinement process can lead to grain sizes falling in the submicron range, or even <100 nm, thus approaching nano scale. The identification of grains is an important issue, and a very efficient tool for this task is electron back-

scatter diffraction (EBSD). In particular, EBSD measurements can generate a topological orientation map in which orientations are distinguished by a color code.

Currently available commercial orientation mapping software codes permit one to identify “grain” boundaries using an imposed condition of minimum misorientation from pixel-to-pixel orientation measurements (for example, Channel5 from HKL Technology, TSL from EDAX). From these boundaries, contiguous regions formed by continuous closed boundaries can be defined; they are usually called grains if the minimum misorientation between the regions on the two sides of a boundary is sufficiently large (commonly 5–15°) (a low value of 2° is commonly used for misorientation frequency analyses). Note that, owing to the large plastic strain in SPD processing, the initial grain boundaries (GB) cannot be distinguished from the new boundaries that are induced by the deformation process.

* Corresponding author. Tel.: +33 3 87 547238; fax: +33 3 87 315366.
E-mail address: toth@univ-metz.fr (L.S. Tóth).

Average orientations can also be assigned to the grains obtained as the averages over the orientations of the pixels that form the grain. Then the misorientation between two adjacent grains can be calculated from their average orientations. It is also of great importance to analyse the distribution density function $\nu(\theta)$ of the misorientation angle θ of the grains that constitute the measured orientation map. Two types of distributions are of interest: the so-called correlated and uncorrelated distributions. The correlated one is defined in terms of the distribution density function of misorientations between neighboring grains, while the non-correlated one is calculated on the basis of misorientations between grains randomly selected from the grain population. In the present work, the correlated distribution will be named the next-neighbor misorientation density (NNMD) function. Mackenzie [2] calculated the uncorrelated distribution density function $\nu(\theta)$ for a face-centered cubic (fcc) polycrystal with a random distribution of grain orientations, which is commonly referred to as the “Mackenzie distribution”.

In SPD processing, one of the most important issues is the grain size distribution due to the grain refinement process. Pantleon [3] examined the problem of grain size determination from orientation maps obtained from EBSD. Using a line-intercept method, he analysed the dependence of the “chord”-length distribution on the choice of step size (or pixel size) and the selected threshold value of the misorientation. He also proposed a procedure to separate the experimentally obtained misorientation distribution into a part that describes the misorientations inside a grain and another that presents the misorientations across the GB only (obtained from the adjacent pixels on the GB along an intercept line). He considered the grain-interior misorientation distribution to originate from fluctuations or noise (“irrelevant” distribution), while the grain-boundary type is assumed to be non-correlated between adjacent grains (more exactly between neighboring pixels on the two sides of a boundary). The non-correlated nature of the orientations of adjacent grains was recently questioned with regard to materials refined by SPD: Beausir et al. [4] showed that a scale-invariant correlation exists between the distances between the centers of adjacent grains and the misorientation angle of their average orientations.

The identification of the grain structure after SPD is of importance, as it can provide quantitative measures of the refined microstructure. The grain size distribution and the average orientation of the identified grains can be used directly in polycrystal plasticity modeling. They are readily available in the most widely used commercial orientation imaging software packages. These numerical codes, however, do not necessarily produce the most relevant information about the structure. For example, they do not have the feature of displaying the distribution density function of the identified grain structure; they produce only the distribution density function of the adjacent pixels of the measurement. This information—however useful it may be for certain purposes—is very different from the NNMD

function defined above. An example is displayed in Fig. 1, where both density functions are plotted for Cu deformed in a 90° ECAP die after three passes (the map was taken on the TD plane; the deformation geometry and further experimental conditions are defined in Section 2). The pixel-to-pixel misorientation frequency distribution has a large peak at small angles, while the NNMD-based one, obtained for the identified grains (using the same 5° misorientation threshold), displays a much larger fraction of high angle misoriented grains. It is important to point out further differences in the techniques used to construct these two types of distributions. In the case of pixel-to-pixel methodology, the detected misorientations do not necessarily correspond to a closed GB delineating a grain (even if their distribution is commonly referred to as the “grain-boundary misorientation distribution”). The frequency value is also affected by the length of the detected boundaries as the number of pixel-to-pixel misorientations along a boundary is proportional to its length. In the case of NNMD, the misorientation values are all calculated between identified grains (with closed GB) and each grain (whether small or large) is counted with the same weight. In conclusion, in order to obtain insight into the misorientation frequency of polycrystals, the grain-based NNMD function is more suitable compared with the pixel-to-pixel misorientation distribution, and it will be employed in the present work.

The aim of the present paper is to examine the correlated misorientation distribution density function $\nu(\theta)$ for neighboring grains in a microstructure produced as a result of ECAP. The population of neighboring grains changes substantially, owing to the grain refinement process at large strains. Any given original grain is replaced by a large number of smaller grains, and all these “daughter” grains have their origin within the “parent” grain. For example, if one makes a simplifying assumption of a cube-shaped parent grain being progressively subdivided into smaller cube-shaped grains, such a grain initially 20 μm in size will

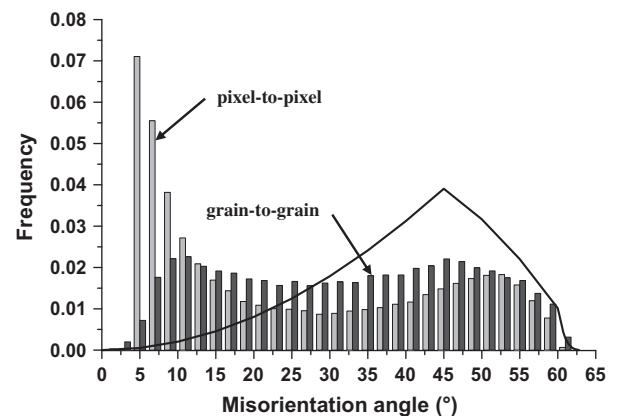


Fig. 1. Comparison between pixel-to-pixel (light gray) and grain-to-grain (dark gray) misorientation distributions (correlated) after three passes of Cu in ECAP on the TD plane. The theoretical Mackenzie distribution (uncorrelated) is plotted by the solid black line.

contain ~ 8000 new grains when the refined grain size goes down to $\sim 1 \mu\text{m}$. The misorientation distribution between these daughter grains is expected to be very different from that associated with the neighbors that are situated across the parent GB, i.e., between grains that stem from different parent grains. When an EBSD measurement is carried out after a high degree of grain refinement, the original GB are not readily distinguishable from the newly emerged ones. Consequently, it appears impossible to obtain a separate misorientation distribution for the “inner” grains, i.e., for those daughter grains within the same parent grain. In the following, a statistical technique is proposed which makes this distinction possible. The importance of obtaining such an intrinsic misorientation function is that it sheds some light on the physics of the grain subdivision process.

2. Experimental

Deformation of OFHC copper by ECAP was carried out in a 90° die at room temperature. The one-pass sample with dimensions $120 \times 20 \times 20 \text{ mm}$ was deformed using the Monash ECAP rig [5] with a cross-head speed of 2 mm s^{-1} . The initial grain size of the material was $24 \mu\text{m}$, and the texture was random. Numerous annealing twins were present in the initial grain structure. The deformed specimen was examined by EBSD on three different sections, ED, TD and ND (extrusion, transverse and normal direction, respectively) of the billet. A specimen was cut from the middle part of the sample and mechanically polished to 4000 grit using SiC paper, and then electropolished for 20 s in an electrolyte of 25% orthophosphoric acid, 25% ethanol and 50% distilled water at 10 V, 20°C with a current of $\sim 150 \text{ mA}$. The EBSD measurements were performed by scanning electron microscopy (SEM) using a JEOL 7001F FEG instrument with a step size of $0.2 \mu\text{m}$. In order to have representative data, three or four maps $80 \times 80 \mu\text{m}$ in size were measured for each plane. X-ray texture was measured on the TD plane using three pole figures on a GBC-MMA texture goniometer.

The three-pass ECAP sample with dimensions $100 \times 10 \times 10 \text{ mm}$ was deformed using the ECAP rig at Metz University [6] at room temperature with a cross-head speed of 1 mm s^{-1} in route A. The initial grain size was $18 \mu\text{m}$, and the texture was nearly random. Annealing twins were also present in the undeformed sample. For EBSD, specimens were prepared from the middle part of the ECAP processed sample on the ED and TD planes. They were first mechanically ground on wet SiC paper (grit 220–2400) with Struers LaboPol-21 followed by electropolishing using Struers Lectropol-5 at 15°C with electrolyte D2 at a polishing voltage of 24 V. The electropolishing was conducted twice for 20 s each time. The EBSD measurements were carried out by SEM on a LEO 1530 FEG instrument with a step size of $0.1 \mu\text{m}$. Automated orientation analyses of the Kikuchi patterns were performed with the Channel5 software package produced by HKL Technology. The map sizes were $80 \times 100 \mu\text{m}$ on the TD and

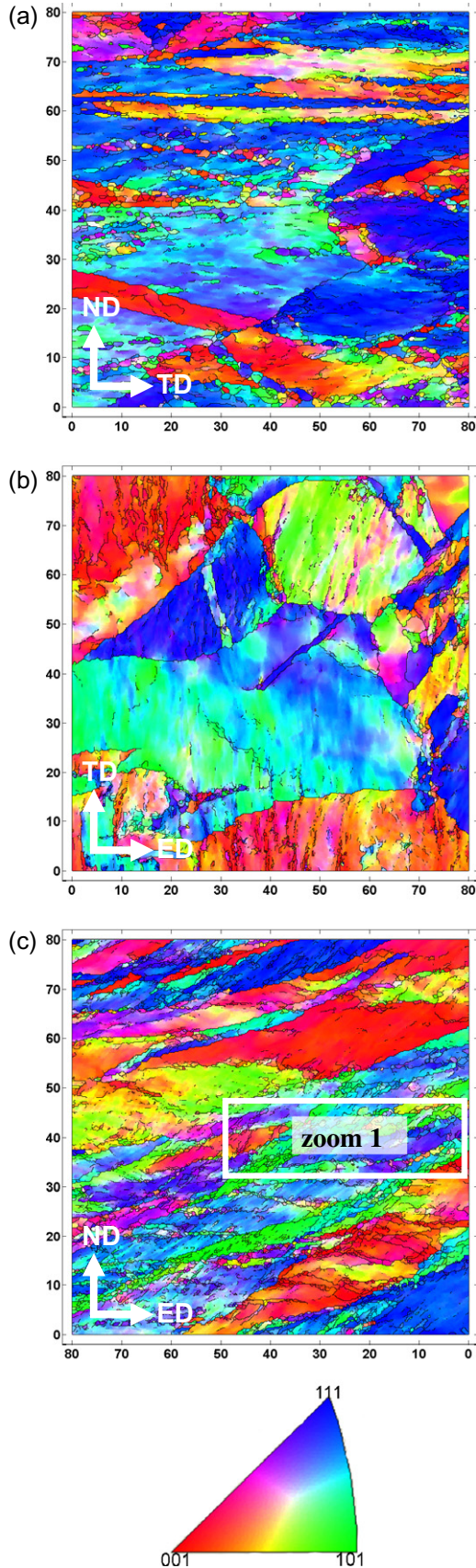
$80 \times 110 \mu\text{m}$ on the ED plane. Texture was measured using synchrotron radiation in the middle part of the sample (for more details see Ref. [7]).

3. Experimental results

Fig. 2 shows examples of EBSD patterns after one-pass ECAP for each plane (one additional map was measured on the TD and three others on the ED plane). For the three-pass ECAP sample, the EBSD maps for two planes (TD and ED) are presented in Fig. 3. These maps are larger and contain more grains (owing to the smaller grain size) than the single maps for the first pass and provide sufficient statistics in terms of the number of grains. Figs. 4a and 5a show the measured NNMD obtained on the ED and TD planes of the one- and three-pass ECAP samples. For the one-pass sample, all measured maps were considered in the construction of the NNMD. The Mackenzie distribution is also traced in Figs. 4a and 5a to enable comparison of the measured NNMD with a random distribution.

It should be emphasized again that the distributions shown in Figs. 4a and 5a were calculated on the basis of misorientations between identified neighboring grains, not between measurement pixels, as is common in the literature, see above. For this purpose, special software was developed [8], which employed the following procedure. First, the misorientation of each pixel with its four (north, south, east and west) neighbors was examined. When the misorientation exceeded the “grain tolerance angle” (here 5°), a boundary was defined. Once all the pixel-based boundaries were defined, a flood-fill procedure was applied to search for sub-areas delimited by a closed boundary. Such sub-areas were defined as grains. Their orientations were defined as an average over the orientations of the pixels composing the grain. Finally, the NNMD between neighbor grains was constructed using these average grain orientations.

Textures in the form of $\{1\ 1\ 1\}$ pole figures measured by the diffraction techniques described above are displayed in Fig. 6a and d for the one- and the three-pass samples, respectively. Similar pole figures were also obtained from the EBSD measurements (see Fig. 6b, c, e and f). All pole figures were projected on the TD plane to facilitate the comparison between them. From a statistical point of view, the pole figures obtained using X-ray or synchrotron radiation (Fig. 6a and d) can be considered as reference measurements. Actually, the displayed textures agree very well with the expected ideal orientations of ECAP textures in Cu [9]. The pole figures obtained from the EBSD measurements all follow the main trends of the reference figures; however, there are also some deviations. This is particularly the case for the one-pass EBSD texture measured on the TD plane. Such differences are good indicators of the quality of the statistically representative nature of the data obtained from EBSD. An EBSD map can be considered to be representative of the microstructure if it yields local textures consistent with the global texture of the material.



4. Split of misorientation distribution

As discussed in Section 1, one can distinguish between two types of correlated grain-to-grain misorientations: (i) those between newly emerged daughter grains that originate within the same parent grain; and (ii) those between daughter grains facing each other across an old GB separating distinct initial parent grains. In accordance with the definitions in Section 1, the first type will be called the “internal” misorientation distribution and will be represented by the function $v_{\text{int}}(\theta)$, while the second type will be referred to as the “old boundary grain” misorientation distribution function, $v_{\text{OBG}}(\theta)$. Fig. 7 schematically illustrates these two populations. The measured total NNMD frequency is

$$v_{\text{total}}(\theta) = f_{\text{int}}v_{\text{int}}(\theta) + f_{\text{OBG}}v_{\text{OBG}}(\theta) \quad (1)$$

Here, f_{int} and f_{OBG} are the fractions of pairs of neighboring grains (a pair being defined as a grain and one of its neighbors) corresponding to the inner (“internal”) grains and to the grains situated at the old GB, respectively. These fractions will be determined below. A very similar decomposition was proposed by Pantleon [3], albeit for another purpose: he examined the pixel-to-pixel misorientation distribution of the grain interiors and the same between the two sides of large angle boundaries. In the present work, grain-to-grain misorientations are examined, as presented in Section 3.

The total number of pairs of grain neighbors N^p contained in the measurement plane indexed by p ($p = \text{ND}, \text{TD}$ or ED) can be calculated as

$$N^p = n_{\text{OG}}^p \left(N_{\text{int}}^p + \frac{1}{2} N_{\text{OBG}}^p \right) \quad (2)$$

where N_{int}^p and N_{OBG}^p are, respectively, the numbers of pairs within the inner part and across the boundaries of a parent grain. n_{OG}^p is the number of the original (or initial) grains covered in the measurement, which is given by $n_{\text{OG}}^p = A_{\text{map}}^p / A_{\text{OG}}^p$, with A_{OG}^p the theoretical area of the parent grains in their deformed state, and A_{map}^p is the map area. The division by 2 in the “OBG” part of Eq. (2) is necessary, as the misorientations across an “old” GB have to be counted only once for a pair of adjoining grains. Dividing by N^p on both sides of Eq. (2) leads to

Fig. 2. Examples of orientation maps after one ECAP pass in pure copper: (a) ED plane; (b) ND plane; (c) TD plane (axis units are in micrometers). Boundaries with at least 5° misorientation are marked with black lines. The color code of the orientations is also shown with the direction of projection perpendicular to the measured plane. The region labeled “Zoom 1” is examined further in Fig. 8. (For interpretation of the references to color in this figure legend, the reader is referred to the web version of this article.)

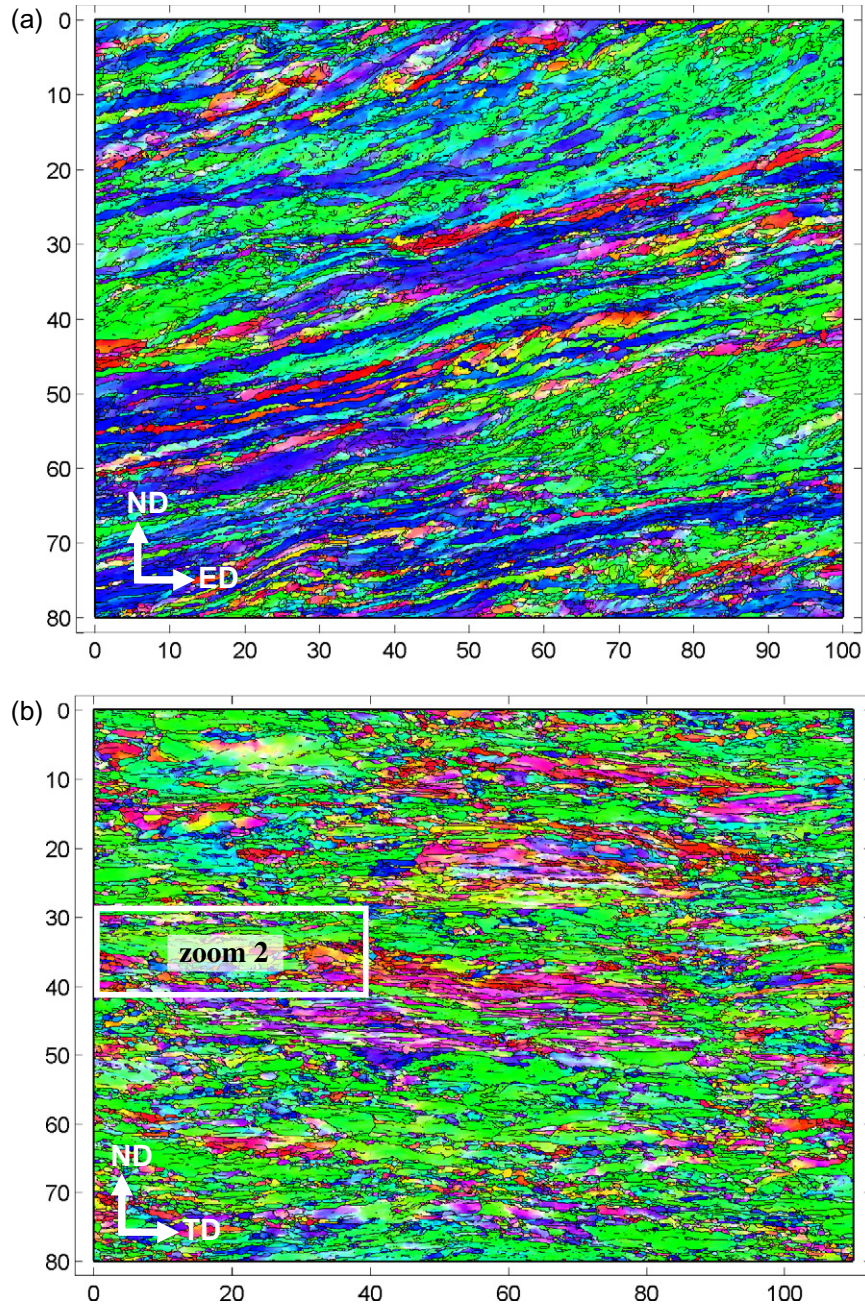


Fig. 3. Orientation maps after three ECAP passes in pure copper: (a) TD plane; (b) ED plane (axis units are in μm). Boundaries with at least 5° misorientation are marked with black lines. The color code is the same as in Fig. 2. The region labelled “Zoom 2” is examined further in Fig. 8. (For interpretation of the references to color in this figure legend, the reader is referred to the web version of this article.)

$$n_{\text{OG}}^p \frac{N_{\text{int}}^p}{N^p} + \frac{n_{\text{OG}}^p}{2} \frac{N_{\text{OBG}}^p}{N^p} = 1 \quad (3)$$

On the basis of this relation, the two fractions (or, in other words, the two weight factors) attributed to the two types of misorientations introduced in Eq. (1) can be defined as

$$f_{\text{int}}^p = n_{\text{OG}}^p \frac{N_{\text{int}}^p}{N^p}, \quad f_{\text{OBG}}^p = \frac{n_{\text{OG}}^p}{2} \frac{N_{\text{OBG}}^p}{N^p} \quad (4)$$

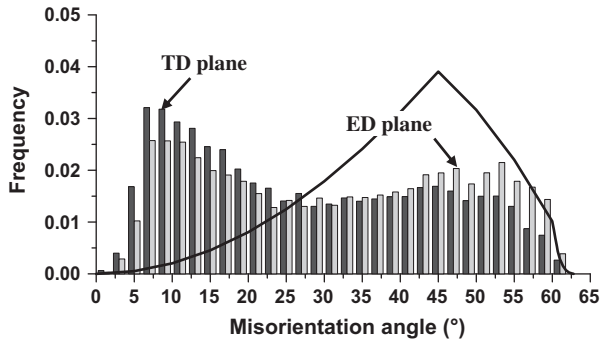
The following relation between the fractions defined above is fulfilled:

$$f_{\text{int}}^p + f_{\text{OBG}}^p = 1 \quad (5)$$

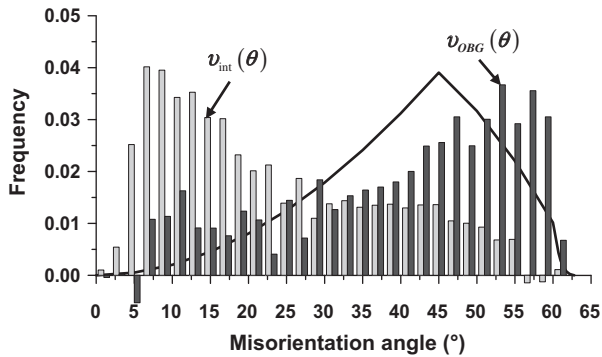
Substitution of N^p from Eq. (2) in Eq. (4) yields the following expressions for the two fractions, or weight functions:

$$f_{\text{int}}^p = \frac{N_{\text{int}}^p}{N_{\text{int}}^p + \frac{1}{2}N_{\text{OBG}}^p}, \quad f_{\text{OBG}}^p = \frac{N_{\text{OBG}}^p}{2N_{\text{int}}^p + N_{\text{OBG}}^p} \quad (6)$$

The relative fractions of the two distributions introduced in Eq. (1) can be calculated from Eq. (6) if N_{int}^p and N_{OBG}^p are known. In the following, a procedure is



(a) Measured total distribution



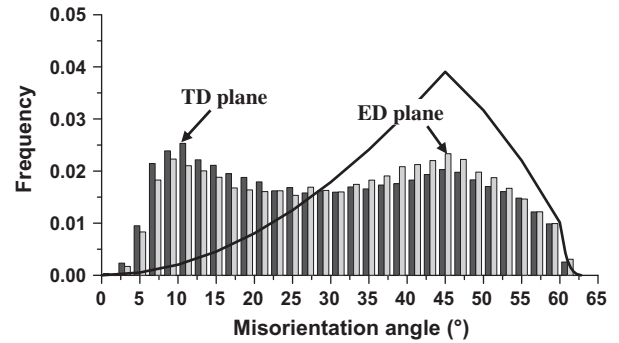
(b) Split distributions

Fig. 4. (a) Experimental neighboring grain misorientation distribution after one ECAP pass for copper obtained on the TD plane (black) and on the ED plane (light gray). (b) The split grain-to-grain misorientation distributions; in light gray the old grain-interior frequency distribution ($v_{\text{int}}(\theta)$) and in dark gray the old boundary layer grain distribution ($v_{\text{OBG}}(\theta)$).

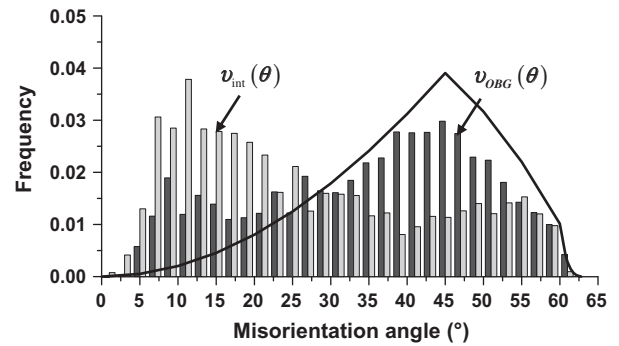
presented which enables a good estimation of these quantities to be obtained. It is sufficient to determine only one of them, as Eq. (2) enables the other to be obtained.

With the new OIM software [8], it is possible to calculate from the experimental EBSD maps the following quantities that are of interest in the present analysis: the average boundary length between two neighboring grains, $\langle l_g^p \rangle$; and the average number of interconnected first neighbors around a grain, $\langle c_g^p \rangle$.

The average boundary length can give the approximate number of new grains located on one side of the original GB by $L_{\text{OGB}}^p / \langle l_g^p \rangle$, where L_{OGB}^p is the average boundary length of the parent grain in its deformed state. The average number of interconnected grains $\langle c_g^p \rangle$ is a parameter borrowed from information technology (network system of computers [10]) which in its present context means the number of neighbors of a grain which are themselves neighbors (or can “communicate with” in its IT meaning). For illustration, some special cases for this quantity are displayed in Fig. 8a. When only one isolated new grain is situated along an original GB, then $\langle c_g^p \rangle = 1$. When a new grain is surrounded at all sides with other new grains in a hexagonal pattern, then $\langle c_g^p \rangle = 6$. Using the quantities defined above, the number of pairs of neighbors for one



(a) Measured misorientation distributions



(b) Split misorientation distributions

Fig. 5. (a) Experimental neighbor-to-neighbor grain misorientation distribution after three ECAP passes in copper obtained on the TD plane (black) and on the ED plane (light gray). (b) The split grain-to-grain misorientation distributions; in light gray the old grain-interior frequency distribution ($v_{\text{int}}(\theta)$) and in dark gray the old boundary layer grain distribution ($v_{\text{OBG}}(\theta)$).

parent grain across its new boundary in the deformed state can be estimated as

$$N_{\text{OGB}}^p = \frac{\langle c_g^p \rangle L_{\text{OGB}}^p}{2 \langle l_g^p \rangle} \quad (7)$$

The division by 2 in Eq. (7) expresses the assumption that, for a given grain in the old GB region, about half the neighbor grains are situated on the opposite side of the initial GB.

One may argue that the above estimation could be used only for a relatively uniform microstructure. Indeed, the EBSD maps, especially at the lower strain (after one ECAP pass) show features of non-uniformity. There are zones that contain few grains and others with many grains. Selected areas taken from the TD section EBSD map of pass one and from the ED section of the three-pass ECAP material are shown in Fig. 8b and c. The dotted lines delineate zones with very different microstructures. Regardless of the number of passes, the microstructure is inhomogeneous. Areas 1 and 4 are quite homogeneous in terms of grain fragmentation. By contrast, Areas 2 and 3 display heterogeneous grain structure exhibiting many incomplete (non-closed) boundaries and a few isolated grains. These inhomogeneities are probably due to the orientation

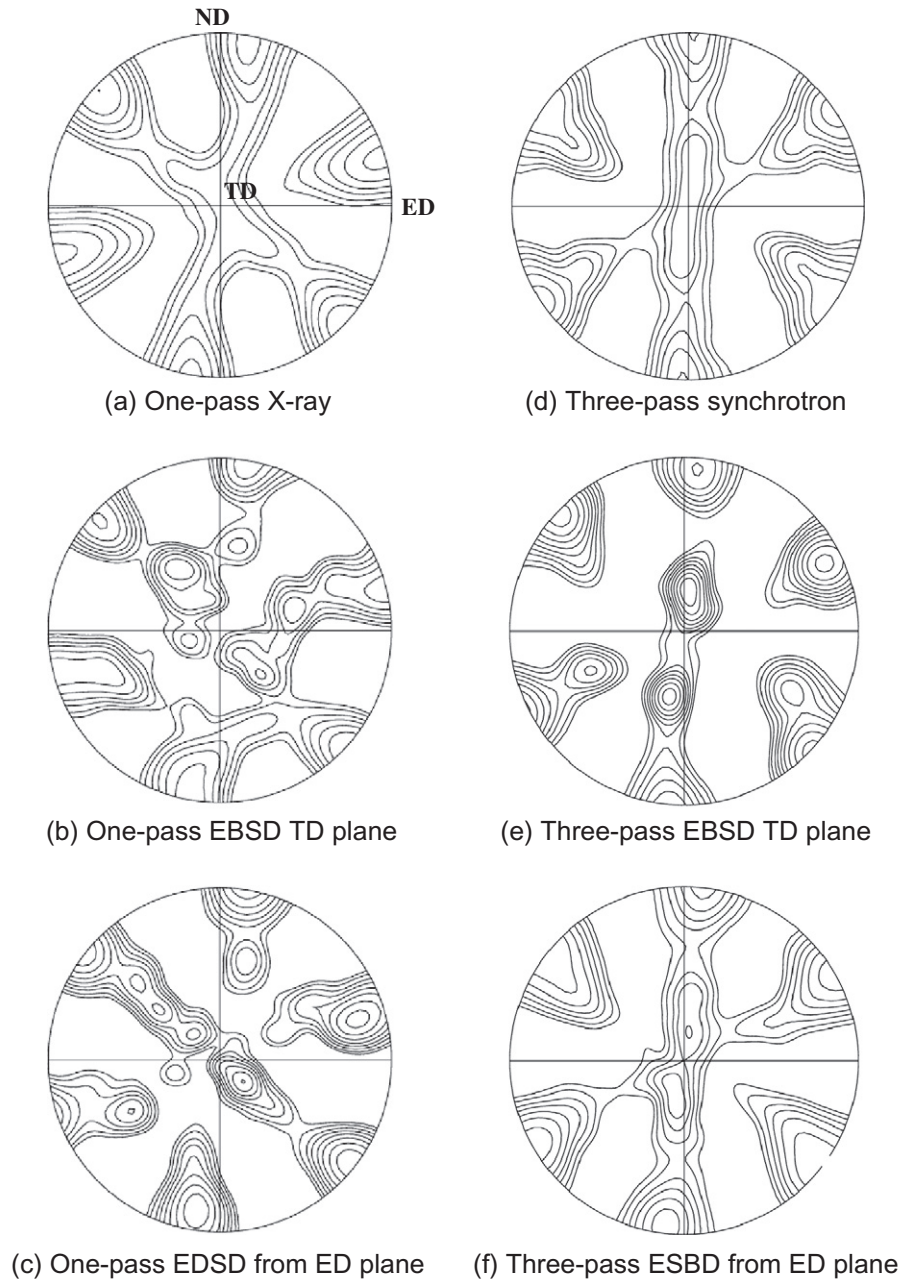


Fig. 6. (1 1 1) pole figures projected on the TD plane of the textures obtained from (a) X-ray diffraction; (b) synchrotron; EBSD after one-pass on (c) TD plane and (e) ED plane; from EBSD after three passes on (d) TD plane and (f) ED plane. Iso-lines: 0.8–1.0–1.3–1.6–2.0–2.5–3.2–4.0–5.0–6.4 (\times random). In all pole figures ED is right, ND is top, and TD is the middle direction.

dependence of the grain fragmentation process; see recent modeling results based on such an assumption in Ref. [11]. These diverse features have a significant effect on the two parameters introduced above, i.e., the number of interconnected neighbors $\langle c_g^p \rangle$, and the average boundary length between two neighboring grains $\langle l_g^p \rangle$, which seem to be able to account for such variability of the microstructures. Both parameters were actually measurement-plane dependent; their numerical values are compiled in Table 1.

The last parameter of the present calculation is the boundary length of the initial (“old”) grain L_{OBG}^p in its deformed state on different plane sections of the sample. It can be

obtained from the geometry of the deformation process if the average initial grain size and the plane of the section are known (see Appendix). The variation in grain size is not considered in the present work, only the average value. In this way, the calculated L_{OBG}^p value is also an average. However, using a single value for the deformed grain size does not mean that the Taylor approach of polycrystal plasticity is adopted in the present work. Individual grains may deform differently. Their average shape, however, always follows the shape change of the macroscopic sample.

Note that all quantities in the above relations can be obtained from the orientation imaging maps and the

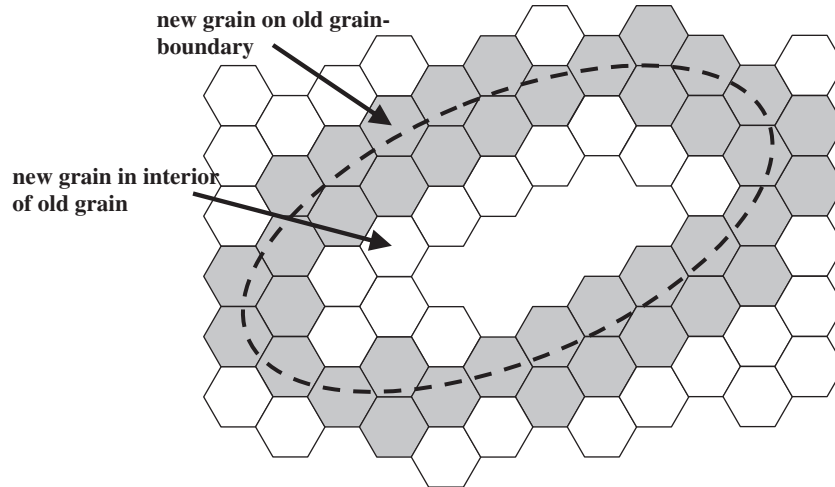


Fig. 7. Schematic showing the trace of a boundary of an “old” grain (broken line) together with the newly emerged, finer grains represented by hexagons. New grains that are sitting at the old GB are shaded.

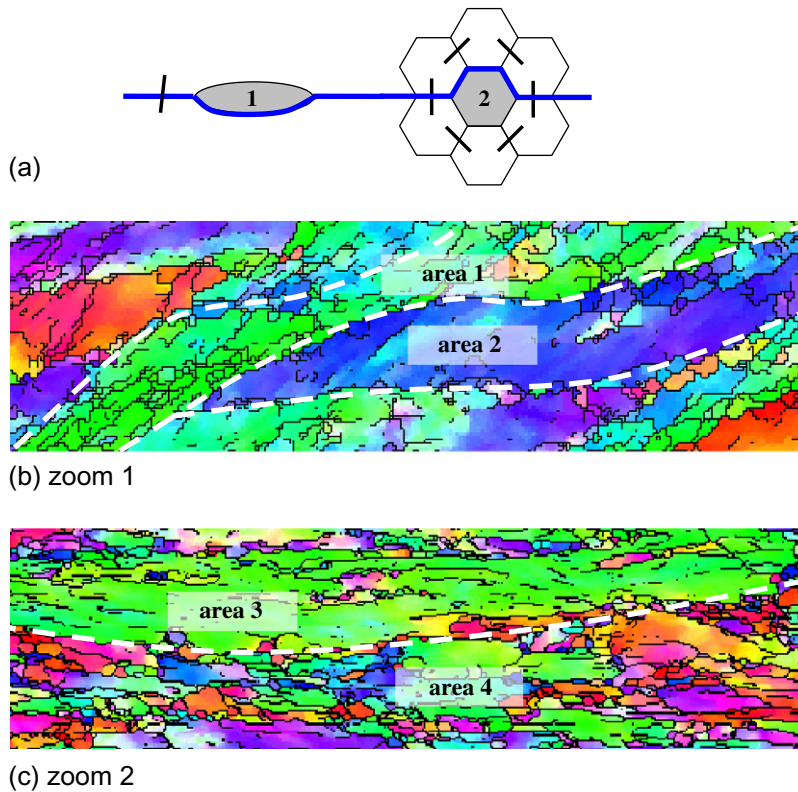


Fig. 8. (a) Schematic illustration of the number of interconnected first neighbors around a grain for two “extreme” cases, the interconnections are indicated by short thick segments, the blue line represents an old GB. (b and c) Zooms in the EBSD map after one-pass ECAP on the TD plane, and after three ECAP passes on the ED plane, respectively. (For interpretation of the references to color in this figure legend, the reader is referred to the web version of this article.)

Table 1

Average boundary length between two neighboring grains, $\langle l_g^p \rangle$, and the average number of interconnected first neighbors around a grain, $\langle c_g^p \rangle$, measured from the EBSD maps on different planes of the one- and three-pass deformed samples; the calculated “internal” as well as the “old boundary grain” type fractions are also indicated.

	$\langle l_g^p \rangle$ on TD (μm)	$\langle l_g^p \rangle$ on ED (μm)	$\langle c_g^p \rangle$ on TD	$\langle c_g^p \rangle$ on ED	$f_{\text{int}}^{\text{TD}}$	$f_{\text{OBG}}^{\text{TD}}$	$f_{\text{int}}^{\text{ED}}$	$f_{\text{OBG}}^{\text{ED}}$
Pass one	1.1	1.6	2.5	5	0.726	0.274	0.509	0.491
Pass three	0.57	0.57	5.4	7.0	0.517	0.483	0.351	0.649

geometry of the process. Now from Eq. (1), the internal part of the NNMD function is expressed as

$$v_{\text{int}}(\theta) = \frac{v_{\text{total}}(\theta) - f_{\text{OBG}}v_{\text{OBG}}(\theta)}{f_{\text{int}}} \quad (8)$$

As mentioned above, two planes were selected for the EBSD measurements: the ED and TD planes. The ND plane was not used here, as the corresponding statistics for old GB-type misorientations was insufficient for that plane. Actually, in route A ECAP testing, the shape of an initial grain remains the same on the ND plane, so that only a small fraction of the new grains are situated along the old GB. In contrast, the flattening process of the initial GB that takes place on the TD and ED planes due to shear increases the relative fraction f_{OBG} of the new grains situating at the old GB. Now it is observed that both $v_{\text{int}}(\theta)$ and $v_{\text{OBG}}(\theta)$ are independent of the plane of measurement. This statement can be made because, in this measurement, one is dealing with two populations of misorientations which are not intermixed. The deviations between the measurements on different planes in Figs. 4a and 5a are due to mixing of the two populations in different proportions, depending on the plane. The misorientation values should not depend on which plane they are measured on, assuming that the orientation of the crystal lattice within a grain is uniform in 3D. Possible non-uniformities within the new grains are neglected in this approach, which is reasonable for the fine-grained structure. Eq. (8) can be used twice for two measurement planes, the ED and the TD:

$$v_{\text{int}}(\theta) = \frac{v_{\text{total}}^{\text{ED}}(\theta) - f_{\text{OBG}}^{\text{ED}}v_{\text{OBG}}(\theta)}{f_{\text{int}}^{\text{ED}}} \quad (9)$$

$$v_{\text{int}}(\theta) = \frac{v_{\text{total}}^{\text{TD}}(\theta) - f_{\text{OBG}}^{\text{TD}}v_{\text{OBG}}(\theta)}{f_{\text{int}}^{\text{TD}}} \quad (10)$$

The distribution density function $v_{\text{OBG}}(\theta)$ can be expressed from Eqs. (9) and (10) as

$$v_{\text{OBG}}(\theta) = \frac{v_{\text{total}}^{\text{ED}}(\theta)f_{\text{int}}^{\text{TD}} - v_{\text{total}}^{\text{TD}}(\theta)f_{\text{int}}^{\text{ED}}}{f_{\text{OBG}}^{\text{ED}}f_{\text{int}}^{\text{TD}} - f_{\text{OBG}}^{\text{TD}}f_{\text{int}}^{\text{ED}}} \quad (11)$$

All quantities entering Eq. (11) are known, which permits $v_{\text{OBG}}(\theta)$ to be calculated. Once $v_{\text{OBG}}(\theta)$ is known, $v_{\text{int}}(\theta)$ is obtained from Eqs. (1) and (9) or (10).

5. Simulation results and discussion

Using the procedure described above, the experimental misorientation functions shown in Figs. 4a and 5a were split into two distributions; the “internal” and the “old boundary grain” types. The results obtained are shown in Figs. 4b and 5b for Cu that went through one and three ECAP passes, respectively.

As can be seen from these figures, the two misorientation distributions are radically different. Within the parent grain interiors, the misorientation frequency is high for low angles, while the misorientations across old GB occur with high frequencies for large angles. Comparing the latter

distribution with the random distribution represented by the Mackenzie curve in Figs. 4 and 5, one can see significant differences. After the first ECAP pass, the measured frequency at misorientation angles around 60° is higher than for the random distribution. This can be attributed to the presence of annealing twins that are typical for copper and only affect that population of misorientations of new grains which border the old GB. This effect disappears at larger strains, as is evident for the third ECAP pass (Fig. 5b). It is also clear that a large population of new grains that have relatively low misorientation angles exists adjacent to the old GB. This may be a result of the development of the texture which promotes such lower misorientation angles [3]. The internal misorientation distribution can also be interpreted in terms of a mechanism of progressive grain subdivision by dislocation cell formation within parent grains with gradual accumulation of misorientation between cells separated by dislocation cell walls. In a recent model of grain refinement [11], when interpreting the obtained misorientation distribution, it was assumed that the part of the misorientation distribution associated with old GB was random. The present results show that such a hypothesis is actually a rather crude approximation.

There are also some negative frequency values which the present analysis returned (cf. Fig. 4b) that need discussion. Of course, such values are unphysical; however, as these distributions were obtained from calculations, this may happen in certain circumstances, as analysis of Eq. (11) shows. With the present experimental data for the one-pass sample (see Table 1), the denominator in Eq. (11) is positive, and hence only a negative value of the numerator can lead to a negative $v_{\text{OBG}}(\theta)$. Again using the experimental values for the weight factors obtained for the one-pass sample, one can see that, for the frequencies to be positive, the difference between $v_{\text{total}}^{\text{ED}}(\theta)$ and $v_{\text{total}}^{\text{TD}}(\theta)$ must not exceed 30% of the smaller of the quantities. This requirement, however, is violated in experiment in some cases. This may be a result of a deficiency in the statistics in a particular range of misorientation angles, meaning that the experimental misorientation distributions obtained on different planes are not fully representative of the microstructure. Section 3 discussed the fact that the textures can be used as indicators of the quality of the statistics, which was not perfectly satisfactory in the EBSD maps for the one-pass sample on the TD plane. Generally, it was estimated that, in order to obtain statistically valid results with the present analysis, at least 10,000 pairs of neighbor grains should be present in an EBSD map for each section. For the one-pass sample maps, the number of grains was 10,473 on the TD plane and 11,589 on the ED plane. Better statistics were achieved for the sample that underwent three ECAP passes, where these numbers were 28,946 and 31,727, respectively.

The technique proposed for deconvoluting the experimental NNMD into grain interior and GB fractions may be of great significance for understanding the mechanism

of grain refinement. For example, in ECAP, the parent grains in the ED section become extremely flat for large numbers of ECAP passes, with the consequence that the fraction of the old GB part of the misorientation function becomes the major element in the total misorientation distribution function. Table 1 shows that, already after the first ECAP pass, the fraction of misorientations across the GB of the parent grains is 49% on the ED plane. This value increases to ~65% after the third pass. Thus, the shift of the total distribution towards large angles can simply be a consequence of the geometry-driven changes in the shape of the parent grains. Such results with respect to the overall misorientation distribution were already observed as early as in 1996 [12]. The situation is different if the material is initially coarse grained or for different strain paths. For example, Iwahashi et al. [13] studied the grain fragmentation in Al by ECAP, starting with a 100 μm grain size and obtained a grain size of 1.3 μm after four ECAP passes in route Bc. For this route, the initial grain shapes are recovered exactly after four passes [14], thus, the fraction of GB misorientations across the GB of the parent grains becomes negligible. In route A, the large initial grain size leads to old GB that are much more separated than those obtained for smaller initial grain sizes; thus, the relative fraction of new grains situated at the old boundaries is smaller. Still, a large fraction of new grains can be present at the old GB, but at a larger strain. For example, for a 100 μm initial grain size, the same effect on the split of the NNMD is expected to be reached after five passes compared with the 24 μm initial grain size material processed in one pass.

It is often claimed that a large number of ECAP passes are needed to increase the fraction of large angle GB. In light of the above considerations, the observed shift towards large misorientation angles in a grain structure is due to the grains adjacent to the GB of the initial grains. In the grain refinement model presented in Ref. [11], it is suggested that fragmentation begins at the GB due to a slow-down of lattice rotation in those regions, which produces lattice curvature. The present analysis supports that hypothesis, providing experimental evidence for large misorientations in the boundary regions of the initial grains. New grains also emerge in the interior of the parent grains, with a misorientation distribution which has a high peak at low angles without showing large development with strain. A comparison of the $v_{\text{int}}(\theta)$ distributions for the one- and three-pass deformed samples in Figs. 4 and 5, respectively, testifies to that. The differences in the misorientation distribution fractions stemming from the two regions (“old boundary” and “internal”) are documented in their characteristics presented in Table 1. For the most part, though, they are due to the geometry variation of the initial grains.

6. Conclusions

The present work has examined in detail the misorientation distribution functions measured on Cu samples

severely deformed by ECAP in route A up to three passes. It has been found that the misorientation distributions depend on the measurement plane. This dependence, as well as other details of the evolution of the misorientation distribution, were interpreted in terms of the geometry changes of the initial grains. The main results of the present studies are as follows:

1. A new statistical type technique was developed which permits the misorientation distribution to be split into the grain interior and the GB related constituents, without the need to identify the old GB in actual experiment.
2. It was shown that the shift in the misorientation distribution towards large misorientation angles caused by grain fragmentation under SPD is mostly due to the geometry changes of the initial grains constituting the polycrystal. Against common belief, the grains emerging in the interior of the parental grains only contribute to small misorientation angles.

Acknowledgements

The authors gratefully acknowledge Dr W. Pantleon (Riso National Laboratory, Denmark) for his constructive remarks made on a previous version of the present paper. This work was funded through an ARC Linkage International Grant (LX0989895). L.S.T. acknowledges an International Fellowship awarded to him as part of this grant and also the University of Metz for granting him a sabbatical leave. B. Beausir is grateful to the Alexander von Humboldt Foundation for his research fellowship.

Appendix A. Relations for grain shape changes in ECAP route A

The dimensions of a deformed initial grain can be obtained from the geometry of the process. The following formulas refer to route A processing. Assuming that the initial form of the grain is spherical, the simple shear process of ECAP transforms it into an ellipsoid. The semi-major axis a and the semi-minor axis b of the corresponding ellipse on the TD plane can be obtained from the following equations:

$$\frac{a}{b} = \frac{1}{2} \left(\gamma^2 + 2 + \gamma \sqrt{\gamma^2 + 4} \right), \quad c^2 = ab \quad (\text{A1})$$

where $\gamma = 2n$ is the total shear strain after n ECAP passes, and $2c$ is the initial grain diameter. On the ED plane, the old GB appear as ellipses with major axes parallel to TD. The semi-minor axis of the ellipse on the ED plane, denoted by l , can be obtained from the following relations:

$$\frac{c}{l} = \sqrt{\frac{b}{a} \sin^2 \alpha + \frac{a}{b} \cos^2 \alpha}, \quad \alpha = \frac{1}{2} \arctg \left(\frac{2}{\gamma} \right) \quad (\text{A2})$$

where α defines the orientation of the ellipse on the TD plane with respect to the ED plane, see Fig. 9. The major

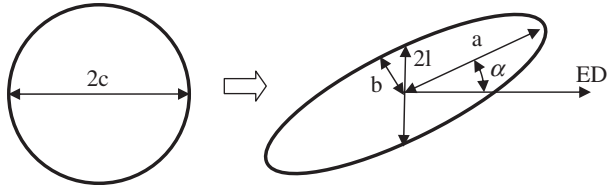


Fig. 9. Geometry of an old grain on the TD plane in ECAP.

semi-axis is given by c on the ED plane. Once the two semi-axes of the ellipse (a and b) are known, the circumference of the ellipse, that is L_{OGB}^P , can be calculated using the approximation of Ramanujan [15] on both the ED and TD planes:

$$L_{\text{OGB}}^P = \pi \left[3(a+b) - \sqrt{(a+3b)(3a+b)} \right] \quad (\text{A3})$$

References

[1] Valiev RZ, Langdon TG. *Progr Mater Sci* 2006;51:881–981.

- [2] Mackenzie JK. *Biometrika* 1958;45:229.
- [3] Pantleon W. *Probl Mater Sci* 2007;52:13–23.
- [4] Beausir B, Fressengeas C, Guroo N, Tóth LS, Suwas S. *Acta Mater* 2009;57:5382–95.
- [5] Lapovok R. *J Mater Sci* 2005;40:341–6.
- [6] Mathieu J-P, Suwas S, Eberhardt A, Tóth LS, Moll P. *J Mater Process Technol* 2006;173:29–33.
- [7] Skrotzki W, Scheerbaum N, Oertel C-G, Arruffat-Massion R, Suwas S, Tóth LS. *Acta Mater* 2007;55:2013–24.
- [8] B. Beausir. Software for orientation image mapping. <<http://benoit-beausir.free.fr/downloads.html>>
- [9] Beyerlein IJ, Tóth LS. *Prog Mater Sci* 2009;54:427–510.
- [10] Strogatz SH. *Nature* 2001;410:268–76.
- [11] Tóth LS, Estrin Y, Lapovok R, Gu C. *Acta Mater* 2010;58:1782–94.
- [12] Mishin OV, Gertsman VY, Valiev RZ, Gottstein G. *Scripta Mater* 1996;35:873–8.
- [13] Iwahashi Y, Horita Z, Nemoto M, Langdon TG. *Acta Mater* 1998;46:3317–31.
- [14] Furukawa M, Iwahashi Y, Horita Z, Nemoto M, Langdon TG. *Mater Sci Eng A* 1998;257:328–32.
- [15] S. Ramanujan. *Ramanujan's collected works*. New York: Chelsea; 1962.